

Article

# Ambient Pressure Synthesis of Re-Substituted MnGe and Its Magnetic Properties

 Vladislav O. Zhupanov <sup>1</sup>, Roman A. Khalaniya <sup>1</sup>, Alexey V. Bogach <sup>2</sup>, Valeriy Yu. Verchenko <sup>1,3</sup> , Maxim S. Likhanov <sup>1</sup>  and Andrei V. Shevelkov <sup>1,\*</sup> 
<sup>1</sup> Department of Chemistry, Lomonosov Moscow State University, 119991 Moscow, Russia

<sup>2</sup> Prokhorov General Physics Institute of the Russian Academy of Sciences, 119991 Moscow, Russia

<sup>3</sup> National Institute of Chemical Physics and Biophysics, 12618 Tallinn, Estonia

\* Correspondence: shev@inorg.chem.msu.ru

**Abstract:** Due to their non-centrosymmetric structure, B20-type compounds have intriguing properties of chiral magnets and are the objects of study of topological spin textures. Among them is a high-pressure phase MnGe, which demonstrates properties of magnetic skyrmions. We report on the synthesis of an  $Mn_{1-x}Re_xGe$  solid solution with the B20 structure, which can be prepared without the application of high pressure.  $Mn_{1-x}Re_xGe$  ( $x = 0.169(6)$ ) shows unconventional magnetic behavior, where the Neel temperature is only slightly reduced compared to a chiral-lattice helimagnet MnGe.

**Keywords:** B20-type structure; manganese monogermanide; magnetic properties; rhenium



**Citation:** Zhupanov, V.O.; Khalaniya, R.A.; Bogach, A.V.; Verchenko, V.Y.; Likhanov, M.S.; Shevelkov, A.V. Ambient Pressure Synthesis of Re-Substituted MnGe and Its Magnetic Properties. *Crystals* **2022**, *12*, 1256. <https://doi.org/10.3390/cryst12091256>

Academic Editors: Patrice Berthod, Grzegorz Golański and Marek Sroka

Received: 21 August 2022

Accepted: 2 September 2022

Published: 5 September 2022

**Publisher's Note:** MDPI stays neutral with regard to jurisdictional claims in published maps and institutional affiliations.



**Copyright:** © 2022 by the authors. Licensee MDPI, Basel, Switzerland. This article is an open access article distributed under the terms and conditions of the Creative Commons Attribution (CC BY) license (<https://creativecommons.org/licenses/by/4.0/>).

## 1. Introduction

Compounds of the cubic FeSi structure type, also known as B20-type, have attracted great attention in recent years [1,2]. The interest in this family of compounds is caused by a special yet simple crystal structure (Figure 1), which leads to intriguing magnetic properties. The cubic unit cell belongs to the  $P2_13$  space group, which does not have an inversion center, rendering the existence of two enantiomeric structures possible. As shown in Figure 1b, iron atoms that do not lie on the [111] axis form spirals that can twist clockwise or counterclockwise, whereas silicon atoms form similar spirals with an inverted rotation. Single crystals of B20-type compounds have enantiomorphic purity, while both forms are present in powdered samples. This group includes monosilicides and monogermanides of various transition metals including chromium, manganese, iron, and cobalt, as well as silicides RuSi, OsSi, RhSi, ReSi, and some other compounds, for example PdE and PtE ( $E = Al, Ga$ ). Of particular interest are the  $3d$  transition metal derivatives capable of exhibiting magnetism in the non-centrosymmetric B20 structure that leads to the appearance of a nontrivial magnetic order—helical magnetic structure, due to the Dzyaloshinsky-Moriya interaction.

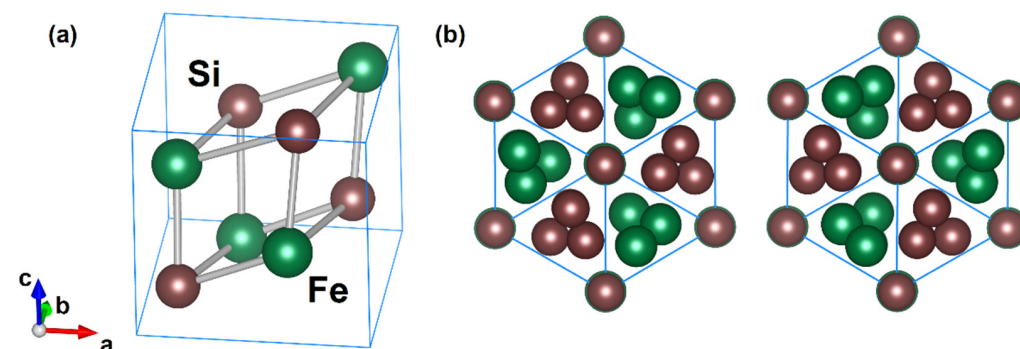


**Figure 1.** Crystal structure of the B20-type FeSi: the unit cell (a) and view of two enantiomers along the [111] axis (b).

There are many studies devoted to chiral magnetism in CrGe [3], MnSi [4,5], CoSi [6,7], and Co- or other metals doped FeSi with very high anomalous Hall conductivity [8,9]. These discoveries are important for spintronics and lead to an active search for materials with nontrivial behaviors [8,10]. Such properties of the B20-type members as helimagnetism, multigap superconductivity, field-induced skyrmion lattices, high-spin to low-spin transition, quantum phase transitions, and chiral topological fermions are widely discussed [6,7,11–14]. Particular attention is drawn to magnetic skyrmions, which were first discovered in MnSi and  $\text{Fe}_{1-x}\text{Co}_x\text{Si}$  [12,15].

In addition to the studies of transitions between the skyrmion-lattice phase and the conventional magnetic order towards development of novel memory devices, studies of transitions between spin textures with different topological order, for example, between the skyrmion and hedgehog-lattices in  $\text{MnSi}_{1-x}\text{Ge}_x$ , are gaining popularity [14]. MnGe and solid solutions on its base are particular materials in the ocean of the B20-type compounds. They demonstrate real-space short-period lattice of skyrmions, transformable antiskyrmions, topological transitions between skyrmion- and hedgehog-lattice states, long-period helical structures and twist-grain boundary phases [14–26].

However, MnGe and its substituted analogs, as well as some other compounds of the B20 structure type, for instance CoGe or RhGe [27,28], can be obtained exclusively under high pressure conditions.

When discussing the transport properties of compounds, the possibility of applying the 18-n rule [29], should be mentioned. Each atom of the transition metal in the B20 crystal structure has six contacts with the same atoms, which provides the valence electron count equal to  $\text{VEC} = 18 - 6 = 12$ , necessary for the implementation of semiconducting properties. Indeed, group eight metal silicides, FeSi, RuSi, and OsSi, exhibit non-metallic properties, while a deviation from the  $\text{VEC} = 12$  induces a metallic state [30]. Separately, we note that the replacement of silicon by heavier germanium in FeSi also leads to the collapse of the band gap and, as a consequence, metallic conductivity. MnGe exhibits metallic properties, however, a transition to the semiconducting state is observed, when manganese is substituted by rhodium  $\text{Mn}_{1-x}\text{Rh}_x\text{Ge}$  in the concentration range of  $0.3 \leq x \leq 0.7$  [20].

In this work, we show that the high-pressure compound, MnGe, can be stabilized at the ambient pressure by the partial substitution of rhenium for manganese, which leads to the  $\text{Mn}_{1-x}\text{Re}_x\text{Ge}$  solid solution with a narrow homogeneity range of  $0.16(2) < x < 0.20(2)$ . We report on the synthesis, crystal structure, and magnetic properties of the new solid solution.

## 2. Materials and Methods

### 2.1. Synthesis

All syntheses were carried out using manganese (99.95%, Alfa Aesar (Ward Hill, MA, USA)), rhenium (99.99%, Alfa Aesar), and germanium (99.999%, Sigma-Aldrich (Burlington, MA, USA)) powders. Powders of metals and germanium were placed in corundum crucibles, which were enclosed in quartz ampoules. The ampoules were evacuated (residual pressure of  $\sim 1 \cdot 10^{-3}$  Torr) and sealed off. Samples with the nominal composition of  $\text{Mn}_{1-x}\text{Re}_x\text{Ge}$  ( $x = 0.15, 0.17, 0.2, 0.25, 0.4, 0.75$ ) were obtained in polycrystalline form by annealing in the following regime: heating to 950 °C at a rate of  $\sim 100^\circ/\text{h}$  for 2 days for primary homogenization of reagents, cooling to 750 °C within 6–7 h, and holding for 5 days at this temperature. After cooling in the shut-off furnace, the ampoules were unsealed, and the resulting samples were carefully ground in an agate mortar, then pressed into cylindrical pellets, which were placed in quartz ampoules and sealed off. The secondary annealing was carried out by heating up to 750 °C and holding for one week. The samples obtained after the second annealing were also ground into fine powders, which were used for further investigation.

### 2.2. Characterization

Phase composition of all powdered samples was determined by powder X-ray diffraction (PXRD) analysis using a Huber G670 Guinier Camera (Cu  $K\alpha_1$  radiation, Ge monochro-

mator,  $\lambda = 1.5406 \text{ \AA}$ ). The data were collected by scanning the image plate 4 times after an exposure time of 2400 s at room temperature.

Elemental composition of the samples was determined on the pellets using a scanning electron microscope, JSM JEOL 6490-LV, equipped with an energy dispersive X-ray (EDX) analysis system, INCA x-Sight. The accelerating voltage was 30 kV. The uncertainty of the measurements for each element was about 1%.

### 2.3. Crystal Structure Investigation

Crystal structure was investigated by PXRD (Figure 2) on a BRUKER D8 Advance diffractometer (Cu  $K\alpha$  radiation,  $\lambda = 1.540593, 1.544427 \text{ \AA}$ ). The crystal structure of the main cubic phase of samples  $\text{Mn}_{1-x}\text{Re}_x\text{Ge}$  with the nominal composition of  $x = 0.17$  and  $0.20$  was refined using the Rietveld method in the Jana2006 program [31]. Crystallographic data and crystal structure refinement details are shown in Tables 1 and 2.

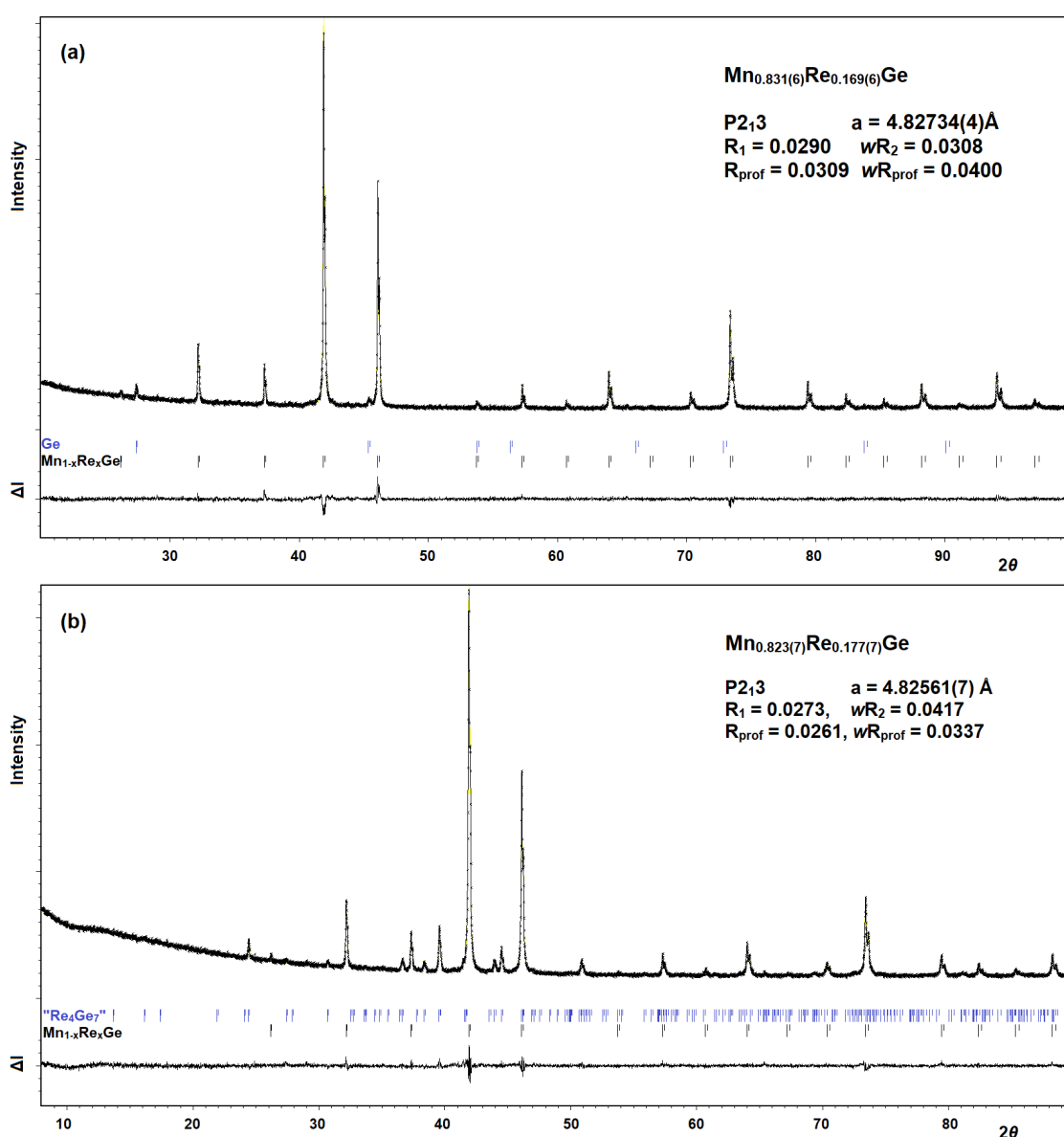


**Figure 2.** Powder X-ray diffraction patterns of  $\text{Mn}_{1-x}\text{Re}_x\text{Ge}$  ( $x_{\text{nominal}} = 0.17$  (a) and  $0.20$  (b)), which correspond to the refined compositions  $x_{\text{refined}} = 0.169(6)$  (a) and  $0.177(7)$  (b). The upper black line represents the experimental diffraction patterns, the ticks show peak positions, and the lower black line is the difference between the experimental and calculated patterns.

**Table 1.** Crystallographic data and structure refinement parameters for the  $Mn_{1-x}Re_xGe$  powder samples.

Sample	$Mn_{1-x}Re_xGe$	
Nominal composition	$Mn_{0.83}Re_{0.17}Ge$	$Mn_{0.80}Re_{0.20}Ge$
Refined composition	$Mn_{0.831(6)}Re_{0.169(6)}Ge$	$Mn_{0.823(7)}Re_{0.177(7)}Ge$
Formula weight, $g \cdot mol^{-1}$	149.73	150.79
Structure type		c-FeSi
Space group		$P2_13$
$a$ , Å	4.82561(7)	4.82734(4)
$V$ , Å <sup>3</sup>	112.372(5)	112.493(3)
$Z$		4
$d_{calc}$ , $g \cdot cm^{-3}$	8.851	8.903
Temperature, K		293
Radiation, $\lambda$ , Å	CuK $\alpha$ , 1.540593, 1.544427	
$2\theta$ range, °	20.0–99.999	8.0–90.001
No. of refined parameters	23	39
$R_1$	0.0290	0.0273
$wR_2$	0.0308	0.0417
GoF	1.27	1.26
$R_{prof}$	0.0309	0.0261
$wR_{prof}$	0.0400	0.0337
Impurity	Ge	"Re <sub>4</sub> Ge <sub>7</sub> "

**Table 2.** Atomic coordinates and thermal displacement parameters for the  $Mn_{1-x}Re_xGe$  powder samples.

Atom	Wyckoff Site	$x/a$	$y/b$	$z/c$	$U_{iso}$ , Å <sup>2</sup>	Occupancy
		$Mn_{0.831(6)}Re_{0.169(6)}Ge$				
M1	4a	0.8655(3)	0.8655(3)	0.8655(3)	0.0051(19)	0.831(6) Mn + 0.169(6) Re
Ge1	4a	0.1575(3)	0.1575(3)	0.1575(3)	0.0098(17)	1
		$Mn_{0.823(7)}Re_{0.177(7)}Ge$				
M1	4a	0.8654(2)	0.8654(2)	0.8654(2)	0.0056(13)	0.823(7) Mn + 0.177(7) Re
Ge1	4a	0.1589(3)	0.1589(3)	0.1589(3)	0.0080(11)	1

#### 2.4. Magnetic Properties

Magnetization of the  $Mn_{0.831(6)}Re_{0.169(6)}Ge$  powdered sample was measured using a Magnetic Properties Measurement System (MPMS-XL5 SQUID, Quantum Design). Measurements were carried out in the zero-field-cooling (ZFC) and field-cooling (FC) conditions in the temperature range of 2–300 K in magnetic fields of 10 mT, 0.1 T, 1 T, and 5 T. Field-dependent magnetization was measured in the ZFC conditions at different temperatures by sweeping magnetic field between  $-5$  T and 5 T.

### 3. Results and Discussion

#### 3.1. Synthesis, Phase Equilibria, and Crystal Structure

All samples with the nominal composition of  $Mn_{1-x}Re_xGe$  ( $x = 0.15, 0.20, 0.25, 0.4,$  and  $0.75$ ) obtained after the second annealing were examined by PXRD. According to the phase analysis, in all samples, the presence of a title compound is observed, the reflections of which are indexed in the  $P2_13$  space group. However, the content of this phase decreases as the rhenium content increases. The most representative diffraction patterns are shown in Figure 3 for the samples with a nominal rhenium content of  $x = 0.15, 0.20,$  and  $0.40$ .

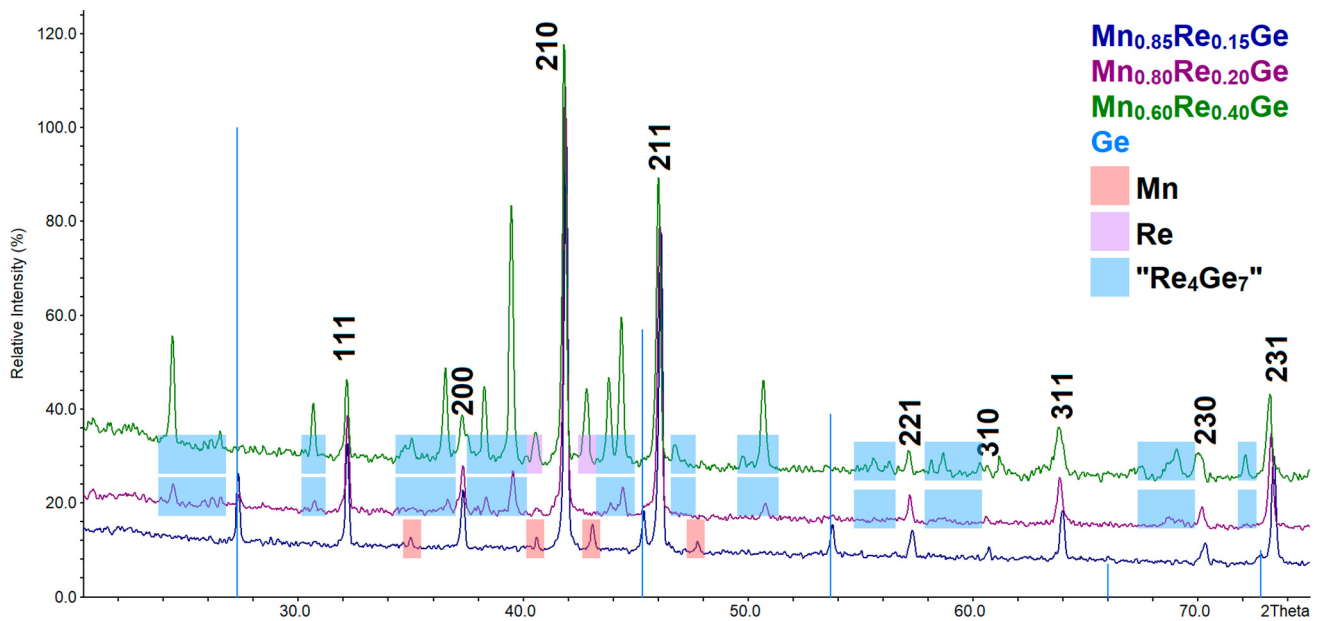


**Figure 3.** PXRD patterns of the  $\text{Mn}_{1-x}\text{Re}_x\text{Ge}$  polycrystalline samples with nominal  $x = 0.15, 0.20,$  and  $0.40$ .

At  $x_{\text{nominal}} = 0.15$ , three phases are in equilibrium—the new cubic compound and elemental manganese and germanium. Here,  $\text{Mn}_{1-x}\text{Re}_x\text{Ge}$  is the main phase. With a further increase of the rhenium content,  $x_{\text{nominal}} \geq 0.2$ , the reflections corresponding to germanium and manganese disappear, but a large set of reflections arises, which, in addition to elemental rhenium, we attribute to a previously unknown compound that is a derivative of the  $\text{Re}_4\text{Ge}_7$  Nowotny chimney ladder phase. Further studies will be devoted to the detailed analysis of “ $\text{Re}_4\text{Ge}_7$ ” phase.

Three powder samples,  $\text{Mn}_{1-x}\text{Re}_x\text{Ge}$  with the nominal composition of  $x = 0.15, 0.20,$  and  $0.40$  were pressed into pellets and their elemental composition was studied (Figure 4). It should be noted that according to the EDX analysis results the composition of the title phase is virtually the same for all samples: Mn:Re:Ge = 43:8:49 at. % ( $x_{\text{nominal}} = 0.15$ ) Mn:Re:Ge = 42:9:49 at. % ( $x_{\text{nominal}} = 0.20$ ) and Mn:Re:Ge = 41:10:49 at. % ( $x_{\text{nominal}} = 0.40$ ), that corresponds to  $\text{Mn}_{1-x}\text{Re}_x\text{Ge}$  with  $x = 0.16(2) - 0.20(2)$ . Mapping of the elements across the surface reveals their homogeneous distribution in the case of  $x_{\text{nominal}} = 0.20$ , whereas for  $x_{\text{nominal}} = 0.15$  and  $0.40$ , a phase contrast is present, which corresponds to the impurity phases, in agreement with the PXRD results. From the results of PXRD and EDX analyses, one can conclude that there is a  $\text{Mn}_{1-x}\text{Re}_x\text{Ge}$  solid solution with a narrow homogeneity range of  $0.16(2) < x < 0.20(2)$ .

We note that this is the first example of the formation of a *hp*-MnGe-based solid solution, which, however, was synthesized without the use of high pressure. All syntheses were carried out at the ambient pressure, and the samples after synthesis remain stable in humid air for an arbitrarily long time.

The main reason of the stability of the new solid solution under normal conditions seems to be the difference in sizes of manganese and rhenium. On the one hand, when replacing manganese with rhenium, we do not violate the formal electronic state, since both elements are in the 7th group of the Periodic Table; on the other hand, the radius of rhenium is much larger than the radius of manganese. However, despite the formal isoelectronic configuration of rhenium and manganese, the *5d*-orbitals of rhenium are more diffuse and, as a rule, rhenium compounds do not exhibit magnetic ordering. It is interesting to study how such a “dilution” of the manganese matrix with rhenium atoms affects the magnetic properties of the solid solution. When discussing the electrically conductive properties of the  $\text{Mn}_{1-x}\text{Re}_x\text{Ge}$  solid solution, we should note that the substitution of manganese for

rhodium does not change the formal valence electron count in any way: Thus, it should be assumed that the  $\text{Mn}_{1-x}\text{Re}_x\text{Ge}$  conductivity remains metallic, as in the parent compound.

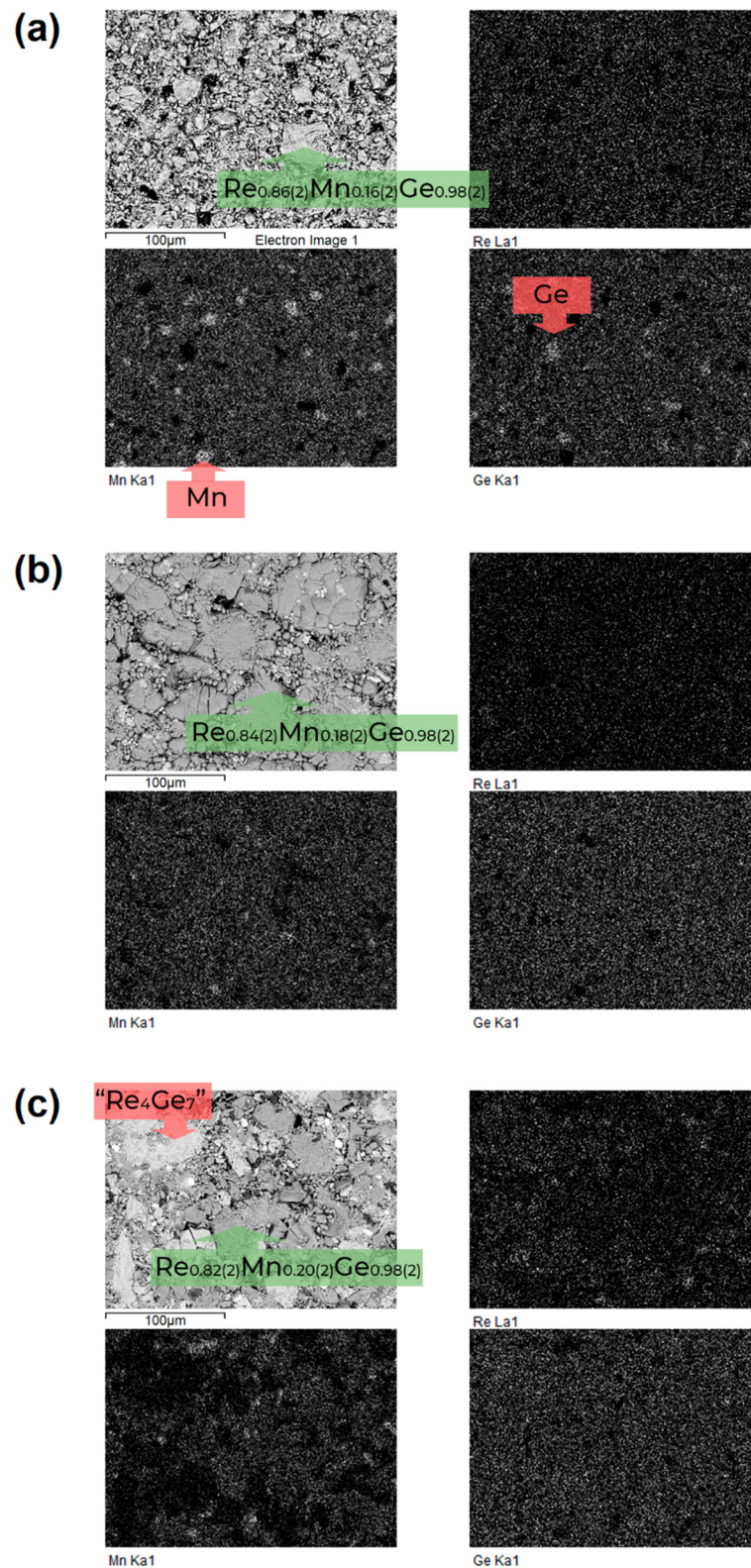


**Figure 4.** EDX mapping of the elements for the samples with nominal ratio of metals:  $\text{Mn}_{0.85}\text{Re}_{0.15}\text{Ge}$  (a),  $\text{Mn}_{0.80}\text{Re}_{0.20}\text{Ge}$  (b), and  $\text{Mn}_{0.60}\text{Re}_{0.40}\text{Ge}$  (c).

The  $\text{Mn}_{0.80}\text{Re}_{0.20}\text{Ge}$  sample ( $x_{\text{refined}} = 0.177(7)$ ) with a minor impurity and the newly synthesized sample with  $x_{\text{nominal}} = 0.17$  ( $x_{\text{refined}} = 0.169(6)$ ) were studied to refine the crystal structure of  $\text{Mn}_{1-x}\text{Re}_x\text{Ge}$ . As expected,  $\text{Mn}_{1-x}\text{Re}_x\text{Ge}$  crystallizes in the cubic FeSi structure type (Space group  $P2_13$ ). In this case, we do not observe any peaks responsible for the formation of a superstructure due to the potential ordering of manganese and rhenium. There are two independent positions in the crystal structure: one for the transition metal (M1) and one for germanium. For the M1 position, the joint population of manganese and rhenium was refined, which turned out to be almost the same in both samples. The crystal lattice parameters for both compositions are also close (see Tables 1 and 2). Also, no anomalies are observed in the values of interatomic distances (see Table 3). They are in the typical range for distances in manganese and rhenium germanides, and marginally increase with increasing rhenium content in the  $\text{Mn}_{1-x}\text{Re}_x\text{Ge}$  solid solution sample.

**Table 3.** Selected interatomic distances in  $\text{Mn}_{1-x}\text{Re}_x\text{Ge}$ .

Atom	Atom	Distance, Å	
		$\text{Mn}_{0.831(6)}\text{Re}_{0.169(6)}\text{Ge}$	$\text{Mn}_{0.823(7)}\text{Re}_{0.177(7)}\text{Ge}$
M1	M1 ( $\times 6$ )	2.958(2)	2.959(1)
M1	Ge1 ( $\times 1$ )	2.441(3)	2.454(2)
M1	Ge1 ( $\times 3$ )	2.514(3)	2.506(2)
M1	Ge1 ( $\times 3$ )	2.718(3)	2.723(2)
Ge1	Ge1 ( $\times 6$ )	2.988(2)	2.992(2)

### 3.2. Magnetic Properties Investigation

Magnetic susceptibility of  $\text{Mn}_{1-x}\text{Re}_x\text{Ge}$  ( $x = 0.169(6)$ ) measured in various magnetic fields is shown in Figure 5a. It exhibits a broad magnetic peak below the characteristic temperature of  $T_N = 145$  K, which was determined using the first-order derivative curve. This peak is gradually suppressed by an increasing magnetic field. The ZFC and FC curves show a bifurcation at low temperatures, where the derivative curve also indicates a minimum at 35 K. Magnetic susceptibility in the paramagnetic state follows the Curie–Weiss behavior (Figure 5b). Fitting the data measured in 1 T magnetic field by the modified Curie–Weiss law  $\chi(T) = \chi_0 + C/(T - \theta)$ , where  $\chi_0$  is the temperature-independent contribution,  $C$ —Curie–Weiss constant, and  $\theta$ —Weiss temperature, yields  $\chi_0 = -0.0067(1)$  emu/mol,  $C = 3.03(2)$  emu K/mol, and  $\theta = 148.6(3)$  K. Similar results were obtained in 5 T magnetic field. The obtained value of Curie–Weiss constant corresponds to the effective moment of  $M_{\text{eff}} = 5.40(1)$   $\mu_B$  per Mn atom. This value is between those of the  $\text{Mn}^{2+}$  and  $\text{Mn}^{3+}$  species, which possess the spin moment of 5.92  $\mu_B$  and 4.91  $\mu_B$ , respectively. The Weiss temperature of  $\theta = 148.6(3)$  K is in agreement with the position of the magnetic peak, and its positive value indicates the ferromagnetic exchange between the magnetic centers.

Field-dependent magnetization of  $\text{Mn}_{1-x}\text{Re}_x\text{Ge}$  ( $x = 0.169(6)$ ) is shown in Figure 5c. At temperatures above  $T_N$ , no remnant magnetization is observed in agreement with the paramagnetic behavior of the compound. Below  $T_N$ , magnetization shows a soft ferromagnetic hysteresis with the absence of saturation even at the lowest measured temperature in the highest magnetic field of 5 T. At  $T = 2$  K, the coercive field of 531 mT is observed accompanied by the magnetization of more than 0.7  $\mu_B$  per f.u. in 5 T magnetic field. The soft low-field ferromagnetic hysteresis and its similarity with that of other B20 compounds [32,33], is consistent with, but not sufficient to determine, a helimagnetic ordered state in  $\text{Mn}_{1-x}\text{Re}_x\text{Ge}$  ( $x = 0.169(6)$ ).

It should be noted that the magnetic properties of  $\text{Mn}_{1-x}\text{Re}_x\text{Ge}$  with  $x = 0.169(6)$  are in good qualitative agreement with those of MnGe [11,34–36], which has the Neel temperature of  $T_N = 170$  K.  $T_N$  is slightly reduced in the case of  $\text{Mn}_{1-x}\text{Re}_x\text{Ge}$  solid solution due to the mixing of Mn and Re atoms in the crystal structure. Notably, similar reduction of  $T_N$  was observed for the  $\text{Mn}_{1-x}\text{Fe}_x\text{Ge}$  solid solution, which shows signatures of a helimagnetic

ordering at low temperatures [36]. The newly discovered  $\text{Mn}_{1-x}\text{Re}_x\text{Ge}$  solid solution may exhibit the helimagnetic properties, too, that fosters its further investigation.

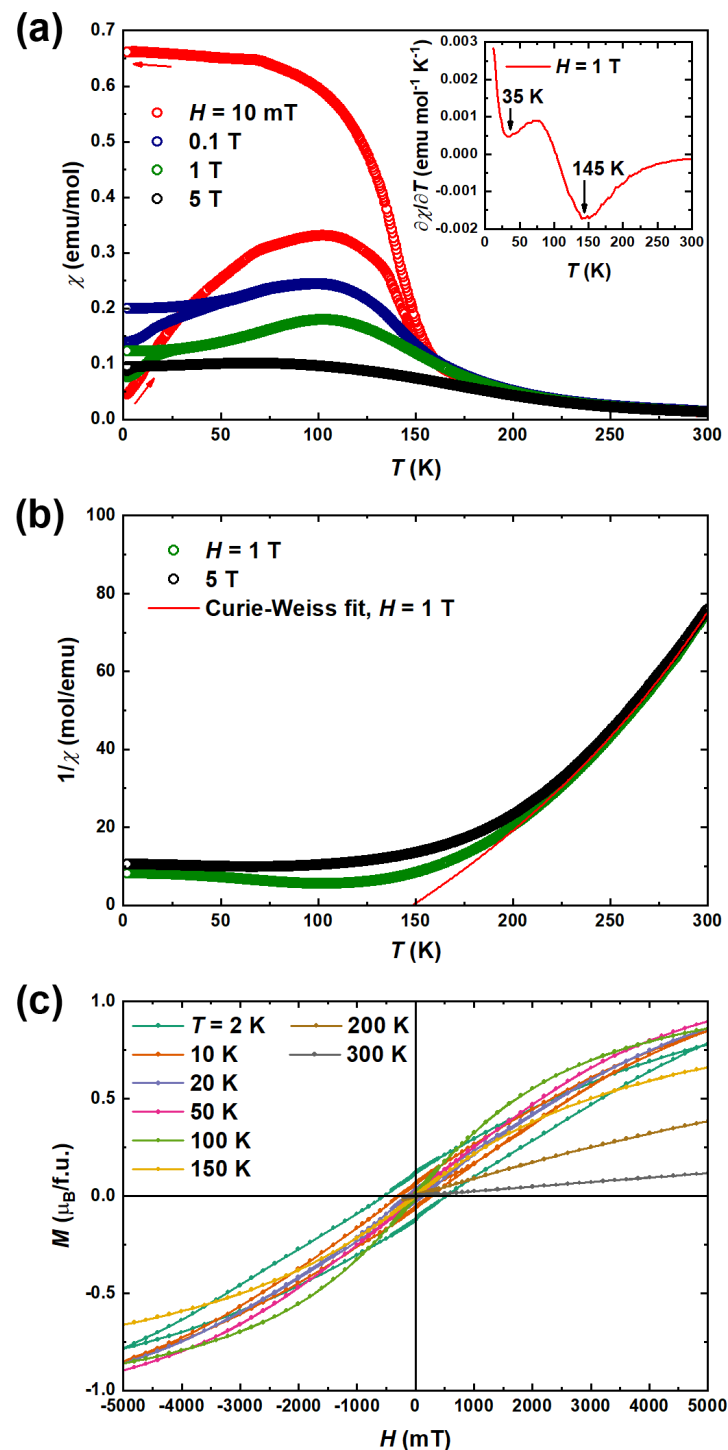


**Figure 5.** Magnetic susceptibility (a), inverse magnetic susceptibility (b) and magnetization (c) of  $\text{Mn}_{1-x}\text{Re}_x\text{Ge}$  ( $x = 0.169(6)$ ). The inset shows a first-order derivative of the ZFC susceptibility in 1 T magnetic field.

#### 4. Conclusions

In summary, a solid solution based on MnGe (B20-type) was synthesized for the first time by substituting part of manganese atoms by rhenium. Unlike previous studies on  $hp$ -MnGe and its solid solutions,  $\text{Mn}_{1-x}\text{Re}_x\text{Ge}$  is synthesized under ambient pressure con-

ditions. The solid solution shows a narrow region of homogeneity ( $0.16(2) < x < 0.20(2)$ ), which is confirmed by a complex of studies including X-ray phase analysis and crystal structure refinement and EDX. An examination of the magnetic properties of the  $\text{Mn}_{1-x}\text{Re}_x\text{Ge}$  ( $x = 0.169(6)$ ) sample shows unusual magnetic behavior similar to the parent compound, indicating possible helimagnetism. However, further studies, including neutron diffraction experiments, are required to accurately establish the nature of the magnetic transition.

**Author Contributions:** Conceptualization, M.S.L. and A.V.S.; formal analysis, V.O.Z., R.A.K., A.V.B., V.Y.V. and M.S.L.; investigation, V.O.Z., R.A.K., A.V.B., V.Y.V. and M.S.L.; writing—original draft preparation, M.S.L.; writing—review and editing, A.V.B., V.Y.V. and A.V.S.; visualization, V.Y.V. and M.S.L.; supervision, A.V.S.; project administration, A.V.S.; funding acquisition, A.V.S. All authors have read and agreed to the published version of the manuscript.

**Funding:** The work was supported by the Russian Science Foundation, grant # 22-13-00006.

**Data Availability Statement:** CCDC 2201883 and 2201884 contain the supplementary crystallographic data for this paper. These data can be obtained free of charge at [www.ccdc.cam.ac.uk/data\\_request/cif](http://www.ccdc.cam.ac.uk/data_request/cif) (accessed on 17 August 2022), by emailing [data\\_request@ccdc.cam.ac.uk](mailto:data_request@ccdc.cam.ac.uk), or by contacting The Cambridge Crystallographic Data Centre, 12 Union Road, Cambridge CB2 1EZ, UK; Fax: +44-1223-336033.

**Conflicts of Interest:** The authors declare no conflict of interest.

## References

1. Tokura, Y.; Kanazawa, N. Magnetic Skyrmion Materials. *Chem. Rev.* **2021**, *121*, 2857–2897. [[CrossRef](#)] [[PubMed](#)]
2. Altynbaev, E.V.; Chubova, N.M.; Grigoriev, S.V. Exotic Spin Structures in Transition-Metal Monosilicides and Monogermanides. *Crystallogr. Rep.* **2022**, *67*, 118–136. [[CrossRef](#)]
3. Klotz, J.; Götze, K.; Förster, T.; Bruin, J.A.N.; Wosnitza, J.; Weber, K.; Schmidt, M.; Schnelle, W.; Geibel, C.; Rößler, U.K.; et al. Electronic band structure and proximity to magnetic ordering in the chiral cubic compound CrGe. *Phys. Rev. B* **2019**, *99*, 085130. [[CrossRef](#)]
4. Nakajima, T.; Oike, H.; Kikkawa, A.; Gilbert, E.P.; Booth, N.; Kakurai, K.; Taguchi, Y.; Tokura, Y.; Kagawa, F.; Arima, T. Skyrmion lattice structural transition in MnSi. *Sci. Adv.* **2017**, *3*, e1602562. [[CrossRef](#)] [[PubMed](#)]
5. Neubauer, A.; Pfleiderer, C.; Binz, B.; Rosch, A.; Ritz, R.; Niklowitz, P.G.; Böni, P. Topological Hall Effect in the A Phase of MnSi. *Phys. Rev. Lett.* **2009**, *102*, 186602. [[CrossRef](#)]
6. Schnatmann, L.; Geishendorf, K.; Lammel, M.; Damm, C.; Novikov, S.; Thomas, A.; Burkov, A.; Reith, H.; Nielsch, K.; Schierning, G. Signatures of a Charge Density Wave Phase and the Chiral Anomaly in the Fermionic Material Cobalt Monosilicide CoSi. *Adv. Electron. Mater.* **2020**, *6*, 1900857. [[CrossRef](#)]
7. Yuan, Q.-Q.; Zhou, L.; Rao, Z.-C.; Tian, S.; Zhao, W.-M.; Xue, C.-L.; Liu, Y.; Zhang, T.; Tang, C.Y.; Shi, Z.-Q.; et al. Quasiparticle interference evidence of the topological Fermi arc states in chiral fermionic semimetal CoSi. *Sci. Adv.* **2019**, *5*, eaaw9485. [[CrossRef](#)]
8. Manyala, N.; Sidis, Y.; DiTusa, J.; Aeppli, G.; Young, D.P.; Fisk, Z. Large anomalous Hall effect in a silicon-based magnetic semiconductor. *Nat. Mater.* **2004**, *3*, 255–262. [[CrossRef](#)]
9. Ou-Yang, T.Y.; Zhuang, Y.C.; Ramachandran, B.; Chen, W.T.; Shu, G.J.; Hu, C.D.; Chou, F.C.; Kuo, Y.K. Effect of Co substitution on thermoelectric properties of FeSi. *J. Alloys Compd.* **2017**, *702*, 92–98. [[CrossRef](#)]
10. Manyala, N.; Sidis, Y.; DiTusa, J.F.; Aeppli, G.; Young, D.P.; Fisk, Z. addendum: Magnetoresistance from quantum interference effects in ferromagnets. *Nature* **2000**, *408*, 616. [[CrossRef](#)]
11. Kanazawa, N.; Onose, Y.; Arima, T.; Okuyama, D.; Ohoyama, K.; Wakimoto, S.; Kakurai, K.; Ishiwata, S.; Tokura, Y. Large Topological Hall Effect in a Short-Period Helimagnet MnGe. *Phys. Rev. Lett.* **2011**, *106*, 156603. [[CrossRef](#)] [[PubMed](#)]
12. Mühlbauer, S.; Binz, B.; Jonietz, F.; Pfleiderer, C.; Rosch, A.; Neubauer, A.; Georgii, R.; Böni, P. Skyrmion Lattice in a Chiral Magnet. *Science* **2009**, *323*, 915–919. [[CrossRef](#)] [[PubMed](#)]
13. Martin, N.; Deutsch, M.; Hansen, T.C.; Fernandez-Diaz, M.T.; Fomicheva, L.N.; Tsvyashchenko, A.V.; Mirebeau, I. Suppression of the bulk high spin-low spin transition by doping the chiral magnet MnGe. *Phys. Rev. B* **2019**, *100*, 060401. [[CrossRef](#)]
14. Fujishiro, Y.; Kanazawa, N.; Nakajima, T.; Yu, X.Z.; Ohishi, K.; Kawamura, K.; Kakurai, K. Topological transitions among skyrmion- and hedgehog-lattice states in cubic chiral magnets. *Nat. Commun.* **2019**, *10*, 1059. [[CrossRef](#)] [[PubMed](#)]
15. Yu, X.Z.; Onose, Y.; Kanazawa, N.; Park, J.H.; Han, J.H.; Matsui, Y.; Nagaosa, N.; Tokura, Y. Real-Space Observation of a Two-Dimensional Skyrmion Crystal. *Nature* **2010**, *465*, 901–904. [[CrossRef](#)] [[PubMed](#)]
16. Martin, N.; Deutsch, M.; Chaboussant, G.; Damay, F.; Bonville, P.; Fomicheva, L.N.; Tsvyashchenko, A.V.; Rössler, U.K.; Mirebeau, I. Long-period helical structures and twist-grain boundary phases induced by chemical substitution in the  $\text{Mn}_{1-x}(\text{Co,Rh})_x\text{Ge}$  chiral magnet. *Phys. Rev. B* **2017**, *96*, 020413. [[CrossRef](#)]
17. Tanigaki, T.; Shibata, K.; Kanazawa, N.; Yu, X.; Onose, Y. Real-Space Observation of Short-Period Cubic Lattice of Skyrmions in MnGe. *Nano Lett.* **2015**, *15*, 5438–5442. [[CrossRef](#)]

18. Iashina, E.G.; Altynbaev, E.V.; Fomicheva, L.N.; Tsvyashchenko, A.V.; Grigorieva, S.V. On the Nature of Defects in Mn<sub>1-x</sub>Fe<sub>x</sub>Ge Compounds Synthesized under High Pressure. *J. Synch. Investig.* **2020**, *14*, 429–433. [[CrossRef](#)]
19. Martin, N.; Deutsch, M.; Itié, J.-P.; Rueff, J.-P.; Rössler, U.K.; Koepf, K.; Fomicheva, L.N.; Tsvyashchenko, A.V.; Mirebeau, I. Magnetovolume effect, macroscopic hysteresis, and moment collapse in the paramagnetic state of cubic MnGe under pressure. *Phys. Rev. B* **2016**, *93*, 214404. [[CrossRef](#)]
20. Sidorov, V.A.; Petrova, A.E.; Chtchelkatchev, N.M.; Magnitskaya, M.V.; Fomicheva, L.N.; Salamatin, D.A.; Nikolaev, A.V.; Zibrov, I.P.; Wilhelm, F.; Rogalev, A.; et al. Magnetic, electronic, and transport properties of the high-pressure-synthesized chiral magnets Mn<sub>1-x</sub>Rh<sub>x</sub>Ge. *Phys. Rev. B* **2018**, *98*, 125121. [[CrossRef](#)]
21. Martin, N.; Mirebeau, I.; Franz, C.; Chaboussant, G.; Fomicheva, L.N.; Tsvyashchenko, A.V. Partial ordering and phase elasticity in the MnGe short-period helimagnet. *Phys. Rev. B* **2019**, *99*, 100402(R). [[CrossRef](#)]
22. Grigoriev, S.V.; Potapova, N.M.; Siegfried, S.A.; Dyadkin, V.A.; Moskvina, E.V.; Dmitriev, V.; Menzel, D.; Dewhurst, C.D.; Chernyshov, D.; Sadykov, R.A.; et al. Chiral Properties of Structure and Magnetism in Mn<sub>1-x</sub>Fe<sub>x</sub>Ge Compounds: When the Left and the Right are Fighting, Who Wins? *Phys. Rev. Lett.* **2013**, *110*, 207201. [[CrossRef](#)] [[PubMed](#)]
23. Altynbaev, E.; Martin, N.; Heinemann, A.; Fomicheva, L.; Tsvyashchenko, A.; Mirebeau, I.; Grigoriev, S. Onset of a skyrmion phase by chemical substitution in MnGe-based chiral magnets. *Phys. Rev. B* **2020**, *101*, 100404. [[CrossRef](#)]
24. Kamaeva, L.V.; Chtchelkatchev, N.M.; Suslov, A.A.; Magnitskaya, M.V.; Tsvyashchenko, A.V. Structural and thermal stability of B20-type high-pressure phases FeGe and MnGe. *J. Alloys Compd.* **2021**, *888*, 161565. [[CrossRef](#)]
25. Skanchenko, D.O.; Altynbaev, E.V.; Martin, N.; Salamatin, D.A.; Sadykov, R.A.; Tsvyashchenko, A.V.; Grigoriev, S.V. Magnetic structure of Mn<sub>0.9</sub>Fe<sub>0.1</sub>Ge compound under quasi-hydrostatic pressure. *J. Alloys Compd.* **2021**, *862*, 158606. [[CrossRef](#)]
26. Repicky, J.; Wu, P.-K.; Liu, T.; Corbett, J.P.; Zhu, T.; Cheng, S.; Ahmed, A.S.; Takeuchi, N.; Guerrero-Sanchez, J.; Randeria, M.; et al. Atomic-scale visualization of topological spin textures in the chiral magnet MnGe. *Science* **2021**, *374*, 1484–1487. [[CrossRef](#)] [[PubMed](#)]
27. Tsvyashchenko, A.V.; Sidorov, V.A.; Petrova, A.E.; Fomicheva, L.N.; Zibrov, I.P.; Dmitrienko, V.E. Superconductivity and magnetism in noncentrosymmetric RhGe. *J. Alloys Compd.* **2016**, *686*, 431–437. [[CrossRef](#)]
28. Salamatin, D.A.; Tsvyashchenko, A.V.; Salamatin, A.V.; Velichkov, A.; Magnitskaya, M.V.; Chtchelkatchev, N.M.; Sidorov, V.A.; Fomicheva, L.N.; Mikhin, M.V.; Kozin, M.G.; et al. Hyperfine field studies of the high-pressure phase of noncentrosymmetric superconductor RhGe (B20) doped with hafnium. *J. Alloys Compd.* **2021**, *850*, 156601. [[CrossRef](#)]
29. Yannello, V.J.; Fredrickson, D.C. Generality of the 18-n Rule: Intermetallic Structural Chemistry Explained through Isolobal Analogies to Transition Metal Complexes. *Inorg. Chem.* **2015**, *54*, 11385–11398. [[CrossRef](#)]
30. Likhonov, M.S.; Shevelkov, A.V. Intermetallic compounds with non-metallic properties. *Russ. Chem. Bull.* **2020**, *69*, 2231–2250. [[CrossRef](#)]
31. Petříček, V.; Dušek, M.; Palatinus, L. Crystallographic Computing System JANA2006: General features. *Z. Kristallogr.—Cryst. Mater.* **2014**, *229*, 345–352. [[CrossRef](#)]
32. Wernick, J.H.; Wertheim, G.K.; Sherwood, R.C. Magnetic behavior of the monosilicides of the 3d-transition elements. *Mater. Res. Bull.* **1972**, *7*, 1431–1441. [[CrossRef](#)]
33. Ludgren, L.; Beckman, O.; Attia, V.; Bhattacharjee, S.P.; Richardson, M. Helical Spin Arrangement in Cubic FeGe. *Phys. Scr.* **1970**, *1*, 69–72. [[CrossRef](#)]
34. DiTusa, J.F.; Zhang, S.B.; Yamaura, K.; Xiong, Y.; Prestigiacomo, J.C.; Fulfer, B.W.; Adams, P.W.; Brickson, M.I.; Browne, D.A.; Capan, C.; et al. Magnetic, thermodynamic, and electrical transport properties of the noncentrosymmetric B20 germanides MnGe and CoGe. *Phys. Rev. B* **2014**, *90*, 144404. [[CrossRef](#)]
35. Tsvyashchenko, A.V.; Sidorov, V.A.; Fomicheva, L.N.; Krasnorussky, V.N.; Sadykov, R.A.; Thompson, J.D.; Gofryk, K.; Ronning, F.; Ivanov, V.Y. High Pressure Synthesis and Magnetic Properties of Cubic B20 MnGe and CoGe. *Solid State Phenom.* **2012**, *190*, 225–228. [[CrossRef](#)]
36. Altynbaev, E.V.; Sukhanov, A.S.; Siegfried, S.-A.; Dyadkin, V.A.; Moskvina, E.V.; Menzel, D.; Heinemann, A.; Schreyer, A.; Fomicheva, L.N.; Tsvyashchenko, A.V.; et al. Doping-induced temperature evolution of a helicoidal spin structure in the MnGe compound. *J. Synch. Investig.* **2016**, *10*, 777–782. [[CrossRef](#)]